The Astrophysical Journal, 653:1510–1516, 2006 December 20
© 2006. The American Astronomical Society. All rights reserved. Printed in U.S.A.

A COMPARISON BETWEEN GLOBAL SOLAR MAGNETOHYDRODYNAMIC AND POTENTIAL FIELD SOURCE SURFACE MODEL RESULTS

Pete Riley, J. A. Linker, Z. Mikić, and R. Lionello
Science Applications International Corporation, San Diego, CA 92121; pete.riley@saic.com, lionelr@saic.com, mikicz@saic.com, linkerj@saic.com

and

S. A. Ledvina and J. G. Luhmann
Space Science Laboratory, University of California, Berkeley, CA 94720; ledvina@ssl.berkeley.edu, jgluhman@ssl.berkeley.edu
Received 2006 July 7; accepted 2006 August 18

ABSTRACT

The large-scale, steady-state magnetic field configuration of the solar corona is typically computed using boundary conditions derived from photospheric observations. Two approaches are typically used: (1) potential field source surface (PFSS) models, and (2) the magnetohydrodynamic (MHD) models. The former have the advantage that they are simple to develop and implement, require relatively modest computer resources, and can resolve structure on scales beyond those that can be handled by current MHD models. However, they have been criticized because their basic assumptions are seldom met. Moreover, PFSS models cannot directly incorporate time-dependent phenomena, such as magnetic reconnection, and do not include plasma or its effects. In this study, we assess how well PFSS models can reproduce the large-scale magnetic structure of the corona by making detailed comparisons with MHD solutions at different phases in the solar activity cycle. In particular, we (1) compute the shape of the source surface as inferred from the MHD solutions to assess deviations from sphericity, (2) compare the coronal hole boundaries as determined from the two models, and (3) estimate the effects of nonpotentiality. Our results demonstrate that PFSS solutions often closely match MHD results for configurations based on untwisted coronal fields (i.e., when driven by line-of-sight magnetograms). It remains an open question whether MHD solutions will differ more substantially from PFSS solutions when vector magnetograms are used as boundary conditions. This will be addressed in the near future when vector data from SOLIS, the *Solar Dynamics Observatory*, and *Solar-B* become incorporated into the MHD models.

Subject headings: solar wind — Sun: magnetic fields

Online material: color figures

1. INTRODUCTION

The two principal approaches for studying the global magnetic structure of the solar corona are (1) potential field source surface (PFSS) models, and (2) magnetohydrodynamic (MHD) models. Both techniques rely on boundary conditions derived from photospheric field measurements. The former have the advantage that they are simple to develop and implement, require relatively modest computer resources, and can resolve global structure on spatial scales beyond those that can be handled by current MHD models. On the other hand, they have been criticized because their basic assumptions (that the field is potential, and that a single, spherical source surface exists) are seldom, if ever, met. In addition, PFSS models cannot directly incorporate time-dependent phenomena, such as magnetic reconnection. PFSS models, however, are used extensively within the solar and heliospheric communities, and thus it is important to assess how well they reproduce the large-scale structure of the corona.

PFSS models, which are essentially an extrapolation of the photospheric field measurements, were first developed in the late 1960s by Altschuler & Newkirk (1969) and Schatten et al. (1969). They solve Laplace's equation within an annular volume above the photosphere in terms of a spherical harmonic expansion, the coefficients of which were derived from the Carrington maps of the photospheric magnetic field (i.e., maps assembled over an entire solar rotation from Earth-based observations). Coronal currents were neglected so as to allow unique solutions in closed form. To circumvent the problem that such simple harmonic expansions would result in all of the magnetic field lines returning to the Sun (i.e., potential solutions), they introduced an outer radial boundary by which point the coronal field was required to become radial (Altschuler & Newkirk 1969; Schatten et al. 1969), leading to what is commonly known as the PFSS model. Above this so-called source surface, typically at 2.5 $R_\odot$, the field is prescribed according to the Parker spiral (Parker 1958). For almost 40 years, PFSS models have been applied to study a wide range of solar and heliospheric topics. These include (1) coronal structure during eclipses (e.g., Smith & Schatten 1970) (2) interplanetary magnetic fields (e.g., Burlaga et al. 1978) (3) wave propagation in the corona (e.g., Uchida et al. 1973) and (4) the photospheric sources of solar wind (e.g., Neugebauer et al. 2002).

Global MHD models are a more recent development. Relying on solutions to more complex equations and requiring significantly more computational power, the first global solutions incorporating observed photospheric fields into the boundary conditions were produced about 10 years ago (Mikić et al. 1996; Usmanov 1996). Although models can be run on single processor machines, the codes in use today (e.g., Linker et al. 1999; Riley et al. 2001; Roussev et al. 2003) typically use the Message Passing Interface (MPI) to run on massively parallel architectures. MHD solutions describe not only the magnetic structure of the corona and solar wind, but also the properties of the plasma. Thus, they can be used to study a wider variety of topics. They have, for example, been used to interpret and connect a wide variety of both solar and in situ observations (e.g., Linker et al. 1999) for specific campaign intervals, as well as to interpret the three-dimensional (3D) results returned by the *Ulysses* spacecraft (Riley et al. 2003a). Of course they can be applied to the

same types of problems for which PFSS models are used (e.g., the solar sources of in situ observations; Riley et al. 2003b).

Since the coronal magnetic field is notoriously difficult to measure, it has proven difficult in the past to directly quantify the accuracy of both PFSS and MHD models. With MHD models, which also compute the coronal density, it is possible to reconstruct simulated white-light images, which then can be directly compared with ground-based and space-based observations. These show that the models can often reproduce the essential large-scale features of the observations.[1] It is also possible to compare the open flux from either model (integrated over a spherical shell) with in situ observations of the interplanetary field (Wang & Sheeley 2002). However, at least for the PFSS model, this is not an independent evaluation, as some of the free parameters have been adjusted to improve the correlation between the data and model output.

To evaluate the accuracy of the PFSS model we have chosen to compare it with MHD simulations. We make no claims that the MHD results are exact reproductions of reality, merely that the additional physics within the MHD model should provide a better solution. This is justified to some extent by eclipse comparisons,[2] as well as direct comparisons with in situ data (Riley et al. 2001; Riley et al. 2002). At the very least, this comparison will allow us to gauge how different the results from the two approaches are, and thus represents an appropriate starting point. Previous studies (e.g., Neugebauer et al. 1998) have compared some aspects of the model results (e.g., loop structure, coronal hole boundaries, and sector crossings) with observations, and these types of comparisons are ongoing (e.g., de Toma 2006).

During the course of the solar cycle, the coronal magnetic field undergoes substantial changes. Near solar minimum, a tilted (or warped) dipole pattern dominates the large-scale structure of the solar corona. Open field lines emanate from large polar coronal holes, and a girdle of closed field lines around the equator defines the streamer belt. At solar maximum, on the other hand, higher order components of the magnetic field can be as large or larger than the dipole term, and the resulting structure is further complicated by the presence of many small-scale active regions. Thus, to properly investigate differences between the two models, we consider comparisons that span the solar activity cycle. In particular, we focus on four Carrington rotations (CRs): CR1910, CR1913, CR1961, and CR1969. The first two occurred at solar activity minimum, while the second two occurred near solar maximum.

For our initial study, we primarily computed PFSS and MHD solutions at relatively low resolution ($61 \times 71 \times 64$ grid points in $r \times \theta \times \phi$). This reflects the fact that we are primarily interested in the large-scale features of the model results and is commensurate with the resolutions typically used by researchers in the field. These runs can be undertaken with modest computing resources. Selected MHD cases were rerun at twice the resolution with no appreciable qualitative differences, demonstrating that our conclusions are not dependent on the resolution of the runs.

The main advantages of the PFSS model are that it is simple to implement and that solutions converge rapidly. The PFSS model does not offer any additional physics that is not contained within the MHD approximation. However, this simplicity comes at a price; it limits the types of problems that can be meaningfully addressed. In particular, there is no time dependence in Laplace's equation, so we are restricted to computing static configurations or a sequence of quasi-static solutions, provided that the boundary conditions do not evolve quickly in time. Thus, the PFSS model cannot address time-dependent processes such as reconnection. On the other hand, it can model the equilibrium states before and after, provided that such states exist at all. Other constraints of the PFSS model include (1) that there exists a spherical source surface, beyond which all field lines are radial (this is typically taken to be between 2.5 and 3.25 $R_\odot$), and (2) the assumption that the magnetic field, particularly around active regions, is potential.

In this paper, we focus on several key assessments of the PFSS model. First, we compare the magnetic structure predicted by both models. Direct comparisons of the magnetic field values at different locations in space, while quantitative, are of limited value, since they do not convey the larger scale structure and connectivity of the field lines. A better approach is to compare the computed coronal hole boundaries. We then use the MHD model to assess one of the fundamental assumptions of most PFSS models, namely, that there exists a spherical surface by which the field becomes radial. Finally, we look at effects due to nonpotential fields, which by definition cannot be addressed within the PFSS approximation, but can be included in the MHD model.

2. BOUNDARY CONDITIONS

Coronal structure is, to a large extent, a consequence of the properties of the magnetic field at the solar surface. In turn, this magnetic field is the result of dynamo effects deep within the Sun that generate bundles of flux that rise and break through the surface, producing bipolar regions (Charbonneau 2005). Although ultimately we would like to understand the physical processes that produce the observed magnetic field at the photosphere, for the purposes of studying coronal structure, a more reasonable and tractable limitation is to set the lower radial boundary of the calculation at the photosphere. This is a natural reference point, as both the line-of-sight and vector magnetic field are readily observable. Moreover, from a physical standpoint, the plasma beta (β, the ratio of gas pressure to magnetic pressure) changes dramatically from $\beta \gg 1$ in the photosphere to $\beta \ll 1$ in the chromosphere.

Beyond $\sim 70^\circ$–75° absolute latitude, constraints imposed by viewing the Sun from the Earth make photospheric measurements difficult. This is further complicated by the modest tilt of the ecliptic plane relative to the solar rotation axis ($\pm 7\overset{\circ}{.}25$), which leads to better observations of one pole at the expense of the other. Thus, determining the polar field strengths can be a significant challenge, and errors can have a significant impact on model solutions (e.g., Hoeksema et al. 1982). This is particularly true at solar minimum, when the polar fields are strongest. Different problems afflict solar maximum solutions; for example, the loss of large polar coronal holes, being replaced by more complex field configurations, makes modeling the structure within polar regions themselves a more difficult task (e.g., Mikić et al. 1999).

3. THE POTENTIAL FIELD SOURCE SURFACE MODEL

In regions where the current density vanishes, the magnetic field is potential and can be derived from a scalar potential (χ) that is subject to Laplace's equation,

$$\nabla^2 \chi = 0. \quad (1)$$

Solutions to equation (1) can be obtained using the method of separation of variables. In spherical coordinates, the general analytic solution is an expansion of spherical harmonics (Schatten

[1] See http://iMHD.net/corona/mar06eclipse/mar06eclipse.html.
[2] See http://iMHD.net/corona/coronal_modeling.html.

et al. 1969; Altschuler & Newkirk 1969). Our PFSS model, which is essentially the potential field solver from the MHD model, relies on a finite difference scheme in all three dimensions. At the inner radial boundary, the radial magnetic field is specified (derived from line-of-sight magnetic field measurements), while at some outer spherical surface, the field is required to be radial. The radius of the outer source surface is a free parameter; however, based on optimizing the computed open flux with in situ measurements of the interplanetary magnetic field, it is usually chosen to be 2.5 $R_\odot$ (Hoeksema et al. 1983). There have been a number of refinements to the PFSS model since its initial application in the late 1960s. Schulz et al. (1978) and Levine et al. (1982), for example, explored the effects of nonspherical source-surface shapes. The effects of current sheets (outside the modeling domain) have also been incorporated (e.g., Zhao & Hoeksema 1995; Wang & Sheeley 1995). However, it is the basic model developed almost 40 years ago that remains the most widely used (e.g., Luhmann et al. 2002), and hence it is this model that we focus our comparison on here. The model used in the Luhmann et al. (2002) paper is available at NASA's CCMC, where it can be "run on demand" using online Wilcox Solar Observatory spherical harmonic coefficients.

4. THE MHD MODEL

We have developed a 3D, time-dependent resistive MHD model to investigate the structure of the solar corona (e.g., Mikić et al. 1999; Linker et al. 1999). We solve the following system of partial differential equations, in spherical coordinates:

$$\nabla \times \boldsymbol{B} = \frac{4\pi}{c}\boldsymbol{J}, \tag{2}$$

$$\frac{1}{c}\frac{\partial \boldsymbol{B}}{\partial t} = -\nabla \times \boldsymbol{E}, \tag{3}$$

$$\boldsymbol{E} + \frac{\boldsymbol{v} \times \boldsymbol{B}}{c} = \eta \boldsymbol{J}, \tag{4}$$

$$\frac{\partial \rho}{\partial t} + \nabla \cdot (\rho \boldsymbol{v}) = 0, \tag{5}$$

$$\rho\left(\frac{\partial \boldsymbol{v}}{\partial t} + \boldsymbol{v} \cdot \nabla \boldsymbol{v}\right) = \frac{1}{c}\boldsymbol{J} \times \boldsymbol{B} - \nabla p + \rho \boldsymbol{g} + \nabla \cdot (\nu \rho \nabla \boldsymbol{v}), \tag{6}$$

$$\frac{\partial p}{\partial t} + \nabla \cdot (p\boldsymbol{v}) = (\gamma - 1)(-p\nabla \cdot \boldsymbol{v} + S), \tag{7}$$

where $\boldsymbol{B}$ is the magnetic field intensity, $\boldsymbol{J}$ is the electric current density, $\boldsymbol{E}$ is the electric field, $\boldsymbol{v}$ is the plasma velocity, ρ is the plasma mass density, p is the gas pressure, $\boldsymbol{g}$ is the acceleration due to gravity, γ is the ratio of specific heats, η is the plasma resistivity, ν is the kinematic viscosity, and S represents energy source terms.

For the purposes of this comparison, we use a relatively simple version of our coronal MHD code. We approximate the energy equation with a simple adiabatic energy equation (i.e., $S = 0$) and choose the polytropic index γ to be 1.05. While this approximation significantly simplifies the calculation and reduces the time necessary to complete a simulation, the resulting plasma parameters predicted by the model do not show the same degree of variation as is inferred from in situ and solar observations. Nevertheless, we have found that the magnetic structure computed using this approximation reproduces the essential features of the corona during solar quiet conditions. We have developed a more complex thermodynamic treatment of the energy equation (Lionello et al. 2001), which promises to yield more realistic plasma parameters; however, for the purposes of this study, its use would unduly complicate the comparisons. We plan to test the effects of improved thermodynamics in a future study.

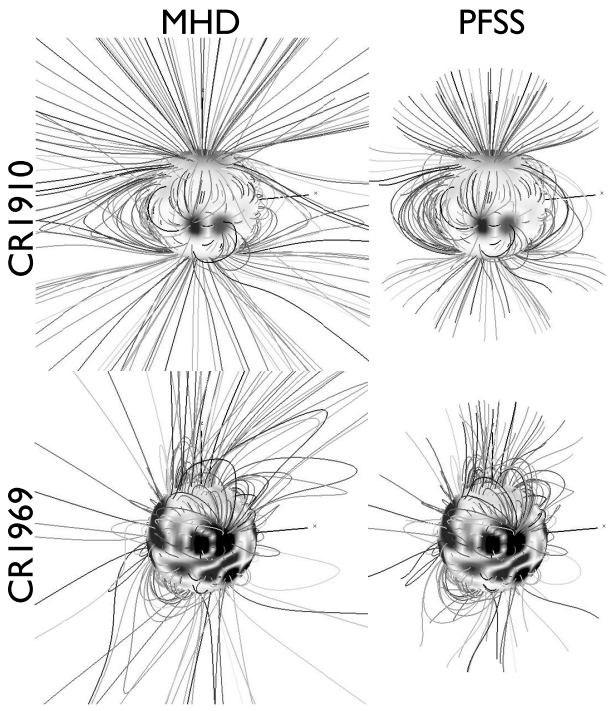

FIG. 1.—Comparison of MHD solution (*left*) with PFSS model (*right*) for Carrington rotations (CRs) 1910 (*top*) and 1969 (*bottom*). The solar surface is colored according to the radial component of the magnetic field at the photosphere. Field lines have been assigned arbitrary colors for ease of identification; however, the same starting points at the photosphere were used in tracing the field lines in all panels, allowing a direct comparison between the PFSS and MHD solutions. [*See the electronic edition of the Journal for a color version of this figure.*]

The details of the algorithm used to advance the MHD equations are provided elsewhere (Mikić & Linker 1994; Lionello et al. 1998). Here we briefly make a few remarks. In the radial (r) and meridional (θ) directions we use a finite difference approach. In azimuth (ϕ) the derivatives are calculated pseudospectrally. We impose staggered meshes in r and θ that have the effect of preserving $\nabla \cdot \boldsymbol{B} = 0$ to within round-off errors for the duration of the simulation.

The coronal calculations are performed between 1 $R_\odot$ (i.e., the base of the corona) and 30 $R_\odot$. At the lower boundary we specify the radial component of the magnetic field, B_r, based on the observed line-of-sight measurements of the photospheric magnetic field and uniform, characteristic values for the plasma density and temperature. This magnetic field profile is identical to that used to compute the PFSS solutions. An initial estimate of the field and plasma parameters are found from a potential field model and a Parker transonic solar wind solution (Parker 1963), respectively. This initial solution is advanced in time until a dynamic, steady-state equilibrium is achieved.

5. COMPARISONS BETWEEN THE PFSS AND MHD MODEL RESULTS

5.1. *The Magnetic Structure of the Corona*

We begin our evaluation of the PFSS and MHD solutions by comparing the magnetic structure predicted by the models at two phases of the solar cycle. The top panels in Figure 1 summarize

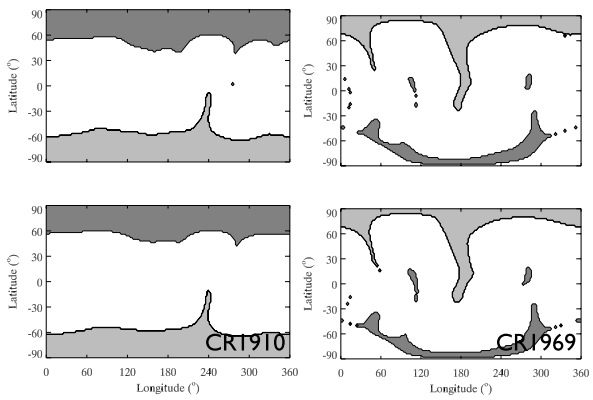

FIG. 2.—Computed coronal hole maps for CR1910 (*left*) and CR1969 (*right*). The MHD and PFSS solutions are summarized in the top and bottom panels, respectively. The coronal holes have been color coded according to the polarity of the magnetic field: red indicates the outwardly directed field, while blue indicates the inwardly directed field. [*See the electronic edition of the Journal for a color version of this figure*.]

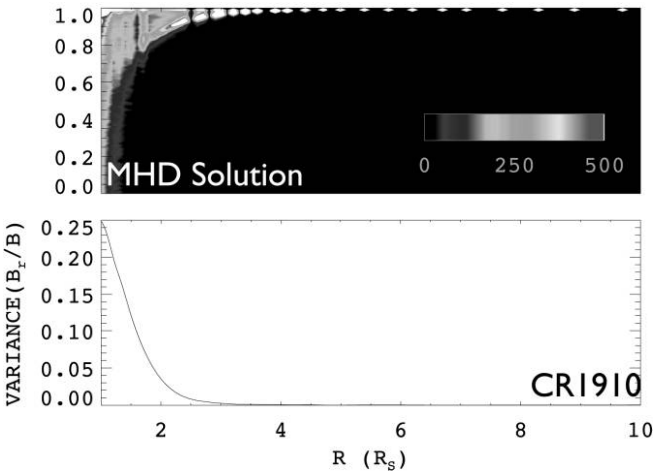

FIG. 3.—Histogram of the number of points, i.e., density of $|B_r|/|B|$ vs. radius for the MHD solution of CR1910 (*top*). The white dots beyond $r = 2$ represent a saturation by all points (at that radius) and are located on the grid points of the simulation. Variance of (B_r/B) vs. radius is also shown (*bottom*). [*See the electronic edition of the Journal for a color version of this figure*.]

the 3D coronal field structure for CR1910, which occurred shortly before the minimum of the solar activity cycle. The bottom panels show the coronal fields for CR1969, occurring around solar maximum. The MHD results are on the left and the PFSS results are on the right. The solar surface is colored according to the radial component of the magnetic field at the photosphere. Field lines have been assigned random colors for ease of identification, and the same starting points at the photosphere were used in tracing the field lines in all four panels. Considering CR1910 first, a comparison between the two panels suggests that, to a first approximation, the PFSS and the MHD model match in a number of respects. The coronal holes (which appear as the bundles of open field lines above the north and south polar regions), for example, are qualitatively the same. The larger, closed loops connecting the northern and southern midlatitudes, as well as the smaller loops associated with the active regions, are qualitatively similar. However, there are several notable differences. First, the PFSS model does not reproduce the cusplike features of the streamer belt, which merge into the heliospheric current sheet in the MHD solution. This can be attributed to the absence of any current sheets either between open and closed field regions or between open field regions. The PFSS model also appears to underestimate the amount of flux opened up to the heliosphere, as inferred from the total number of open field lines. And finally, closed field lines in the PFSS model are, in general, shorter than their MHD counterparts. These inferences also hold true (to a greater or lesser degree) for CR1969.

5.2. *Coronal Hole Boundaries*

An important parameter derived from the magnetic field is the location of the coronal hole boundaries. This is computed by tracing field lines from the solar surface. If they return back to the Sun, then they are closed; if they do not, they are open and are presumably the source of the solar wind. It is implicitly assumed that fast solar wind comes from deeper within large coronal holes, while slow wind may come from the boundaries of large polar coronal holes or from smaller coronal holes (Wang 1994). However, in reality it is quite likely that a process of "interchange reconnection" is taking place, such that the source of the slow solar wind ultimately lies on previously closed field lines (Fisk et al. 1998). Since these field lines are presumably adjacent to already open field lines, the concept of coronal hole boundaries defining the boundary of solar wind flow is still a reasonable one.

In Figure 2 we compare the computed coronal hole boundaries for CR1910 and CR1969. Open field line regions are colored either red (to indicate outwardly directed field lines) or blue (to indicate inwardly directed fields lines). The color white indicates regions of closed field lines. Thus, the coronal hole boundaries are the lines separating white from red/blue regions. While differences can be seen, we infer that the two techniques have reproduced essentially the same qualitative features at both solar minimum and solar maximum. In particular, the polar coronal holes have the same overall shape and span approximately the same area. The only noteworthy differences between the two solutions lie in the area covered by the coronal holes: the PFSS solutions consistently yield smaller coronal holes. This is in agreement with our discussion in § 5.1 and can be understood physically in terms of the pressure exerted by the plasma, which further opens the magnetic field in the MHD simulation. It should be noted that one can adjust the coronal hole areas in the PFSS model results by changing the source surface radius. In fact, Levine et al. (1982) and others experimented with the use of different source surface radii for different phases of the solar cycle.

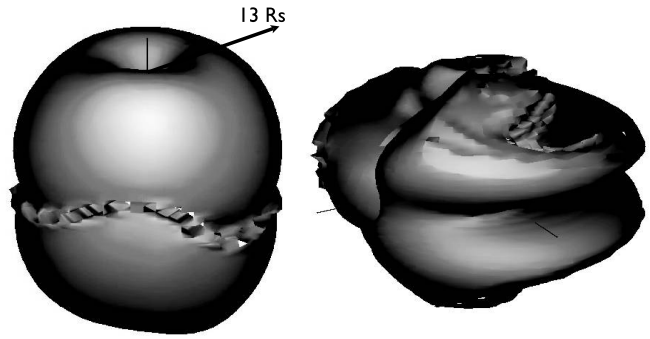

FIG. 4.—Isosurface of $|B_r|/|B| = 0.97$ for the MHD solution of CR1910 (*left*) and CR1969 (*right*). The vertical black line identifies the rotation axis of the Sun. [*See the electronic edition of the Journal for a color version of this figure*.]

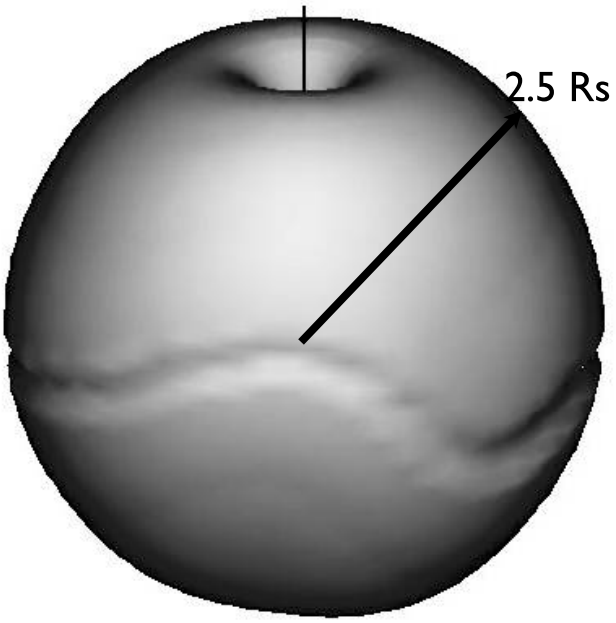

FIG. 5.—Isosurface of $|B_r|/|B| = 0.97$ for the PFSS solution of CR1910. The vertical black line identifies the rotation axis of the Sun. [*See the electronic edition of the Journal for a color version of this figure.*]

5.3. *The Sphericity of Source Surface*

A fundamental assumption of most PFSS models is that the outer boundary is a spherical equipotential. We can use the MHD solutions to test this. In the top panel of Figure 3 we show a 2D histogram (i.e., the density) of $|B_r|/|B|$ points as a function of radius for CR1910. It shows that close to the Sun, the magnetic field can be orientated in essentially any direction (strictly speaking, in this display we cannot distinguish between components in the θ and ϕ directions nor the sign of B_r). However, by 2.5–3 $R_\odot$ the field is essentially radial. The lower plot illustrates the decay in the variance of B_r/B, showing that by 2.5–3 $R_\odot$ it has fallen to $\sim$0.

Figure 3, however, does not retain any information about latitudinal and/or longitudinal variability in the profile of B_r/B with radius. To better assess the assumption that field lines become radial at some spherical shell, we have computed the isosurface of $B_r/B = 0.97$. This is summarized in Figure 4 (*left*) for CR1910. The choice of this numerical value was arbitrary; however, it represents the highest value for which a coherent isosurface could be produced for a range of Carrington rotations.

Thus, at solar minimum, the isosurface assumes the shape of a prolate spheroid (along the rotation axis), with a dimple at each pole. Note that this surface is considerably further away from the Sun (13 $R_\odot$) than the canonical source surface radius (2.5 $R_\odot$). At solar maximum, on the other hand (Fig. 4, *right*), the isosurfaces can show a range of morphologies. Nevertheless, on average they tend to be more spheroidal at solar maximum than at solar minimum. These results are consistent with the work of Zhao et al. (2002), who suggested that the "real" source surface may be located at $\sim$15 $R_\odot$, and may be coincident with the Alfén critical point.

We can also compute the corresponding isosurface for the PFSS results. This is shown in Figure 5. Not surprisingly, it is more spherical than the MHD solution. However, there are two notable deviations. First, there is a sinusoidal variation about the equator, which marks the boundary between the outwardly directed field and inwardly directed field. There are no current

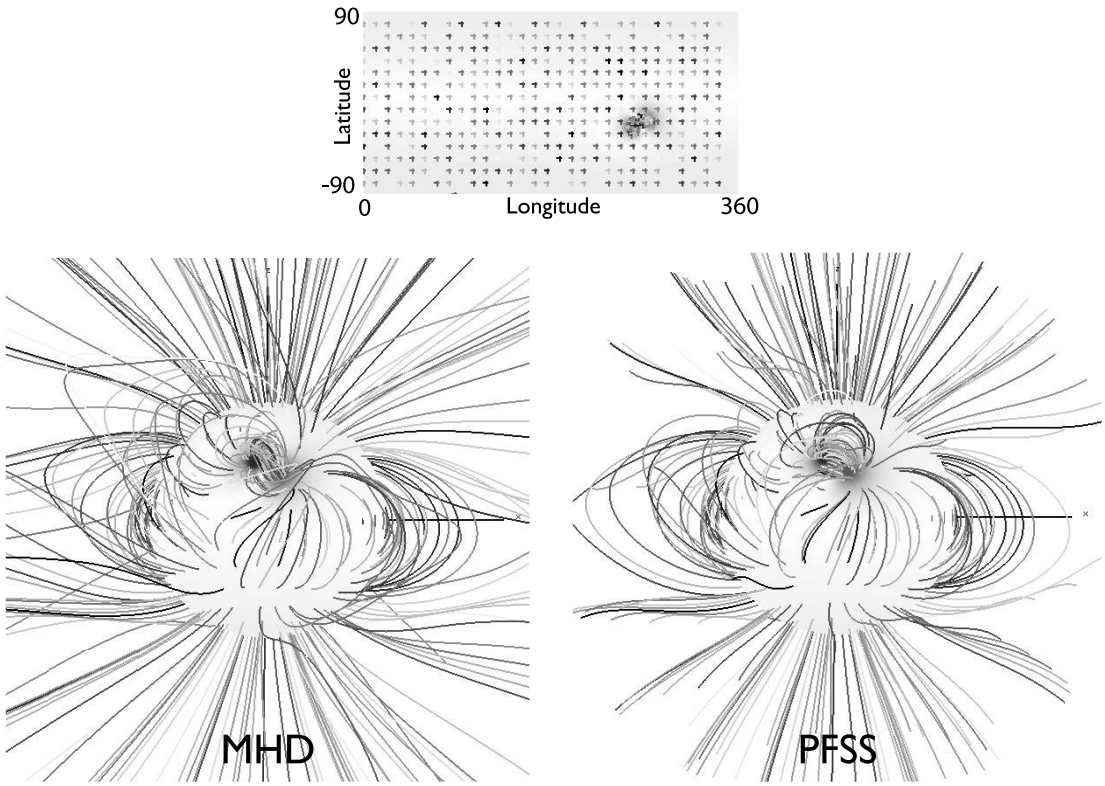

FIG. 6.—Synoptic map (latitude vs. longitude) showing the radial photospheric magnetic field together with a set of field line footpoints (*top*). MHD solution for this boundary condition showing field lines drawn from the footpoints indicated in the top panel are shown at bottom left; same for PFSS solution shown at bottom right. [*See the electronic edition of the Journal for a color version of this figure.*]

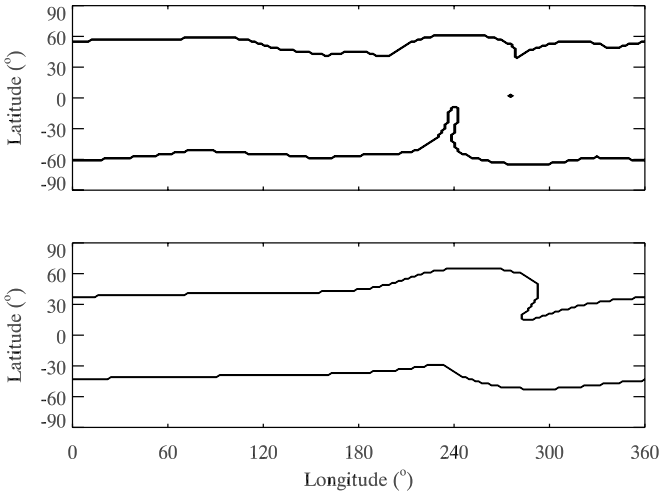

FIG. 7.—Comparison of computed coronal hole boundaries for the MHD solution (*top*) and PFSS solution (*bottom*).

sheets in the PFSS model; however, this is where the neutral line would lie. Second, there are the polar dimples. These represent the fact that while the boundary conditions require that the field becomes radial at 2.5 $R_\odot$, there is no reason that they cannot become radial closer to the Sun.

5.4. *Nonpotential Effects*

We now turn our attention to nonpotential effects. To explore this, we extracted a snapshot from a simulation aimed at exploring the emergence of an active region. During the initial phases of emergence, the solution remains stable. That is, if the emergence is stopped at any time, the configuration does not erupt. We extracted a time slice midway through this early phase as our MHD solution and used the radial component of the magnetic field at this time to construct the PFSS solution. It is important to acknowledge that this configuration is particularly challenging for the PFSS model, since it cannot incorporate any of the temporal history of the emergence, which is present in the MHD solution. Had we rerun the MHD model forward in time using the same radial boundary condition, the solutions would have been much more similar. Moreover, if we allowed the MHD solution to evolve in time with no further flux emergence, it would relax into a configuration resembling the PFSS solution. However, our goal here is to address nonpotential effects (in this case through flux emergence), which can be included in the MHD approach, but not through the PFSS model.

The two solutions are shown in Figure 6. A comparison of the panels again reveals the same large-scale differences in the configuration of the streamer belt. The MHD fields are more inflated, and hence more of them have opened. The outer-most closed fields also display the cusplike morphology that is not present in the PFSS solution. The most striking differences, however, are associated with the active region, where the potential field solution has not captured any of the sheared field lines that are aligned with the neutral line separating the two polarities of the bipole region.

This in itself is perhaps not that surprising; however, the computed coronal hole boundaries in Figure 7 show even more significant differences. In the top panel we show the location of the coronal hole boundaries as deduced from the MHD solution, and in the bottom panel, the PFSS results. The equatorward extensions to the coronal holes are significantly different in the two models; in the MHD solution the southern equatorward extension dominates, whereas in the PFSS solution, it is the northern extension that is larger. Most importantly, the relatively localized emergence of this active region has had a global effect on the location of the coronal holes; whereas the boundaries (away from the active region) lie at $\pm 60^\circ$ latitude in the MHD solution, they lie at $\pm 40^\circ$ in the PFSS solution. We conclude that the presence of nonpotential fields can have significant effects on the coronal hole boundaries.

6. SUMMARY AND DISCUSSION

In this paper we have compared PFSS and MHD solutions of the large-scale structure of the solar corona. We focused on several specific aspects, including the topology of the magnetic field lines, coronal hole boundaries, and the assumptions of the PFSS model (sphericity and potentiality). Our results endorse the PFSS approach, under the right conditions and with appropriate caveats. This will not come as a surprise to many PFSS advocates, yet we hope that this study provides quantifiable support for this position.

The two principal advantages of the PFSS approach are simplicity and speed of execution. However, as computers become faster and MHD models become more user friendly and more generally available to the scientific community (e.g., through the CCMC), these advantages may diminish. Moreover, as more and more physics is incorporated into the MHD models, we may see the solutions diverge more significantly. One important example may come from the use of vector magnetograms to drive the inner boundaries. Clearly, if time-dependent phenomena are important, MHD models will be required. We may, for example, discover that even the basic processes that produce the ambient solar wind are controlled by intrinsically time-dependent processes.

Both the PFSS and MHD models rely primarily on the observed photospheric magnetic field. Line-of-sight measurements of the magnetic field are used to infer the radial component of the field, neglecting any contribution from transverse fields, which can be particularly important in active regions. Moreover, there are subtle, observatory-specific corrections that must be applied to the raw measurements, some aspects of which may not be well understood. It is quite possible that the errors introduced in converting raw magnetograms into radial fields may be as or more significant than whether one chooses to use either the PFSS or MHD model. A comparison of the predicted speed at 1 AU based on magnetic field measurements from three observatories (Wilcox, Kitt Peak, and Mount Wilson) for any given day often shows dramatic differences.[3] PFSS models, which have a number of free parameters (Sheeley 2005), have been "tuned" to account for some of these deficiencies. In particular, comparison of the open flux computed from source-surface solutions with the observed interplanetary magnetic field at 1 AU has been used to constrain some of these parameters.

Plasma boundary conditions in the MHD models have until recently received very little attention. In the simpler MHD models (such as the one used here), which rely on a polytropic equation of state, constant values for temperature and density are prescribed at the inner radial boundary. (Characteristic equations do not allow the user to specify the velocity.) In reality, both temperature and density are expected to vary significantly between closed regions and coronal holes. New MHD models with full thermodynamics are currently completing development (Lionello et al. 2001) and will remove the limitations imposed by the polytropic approximation. However, adding a more complicated description for

[3] See http://sec.noaa.gov/ws/.

energy transport also introduces a new set of unknown parameters. Ultimately, we hope that constraining these parameters by detailed comparisons with narrowband observations will allow us to better understand what processes are at work.

In this analysis, we have chosen a reasonable but necessarily correct set of free parameters for both the PFSS and MHD models. Our generally favorable comparison suggests that they are reasonable values. However, it is well known (e.g., Linker et al. 1999) that the choice of the source surface height influences both the location of the coronal hole boundaries, as well as their shape. In particular, as the source surface height is lowered, the coronal holes tend to become larger. Similarly, in the polytropic MHD model, both the density and temperature and the lower boundary are free parameters. Increasing these parameters leads to a higher kinetic energy density relative to magnetic energy and thus opens up the coronal holes more.

Our results suggest that the source surface is more spherical at solar maximum than at solar minimum, which may seem somewhat surprising. However, during the declining phase and solar minimum, the solar field is dominated by the dipole component. This leads to a more prolate (with major axis along the magnetic dipole axis) shape, and has been accounted for analytically in the generalized PFSS modeling by Schulz et al. (1978). On the other hand, at solar maximum, higher order components of the field become significant, breaking this axial symmetry. While individual active regions can alter the location of the source surface above them, in an average sense, this surface more resembles a sphere.

We have shown that nonpotential effects can have a significant effect on the magnetic structure of the corona. However, our results were based on the idealized evolution of a simple large, active region. From this, it is difficult to infer how important nonpotential effects are in general, but it is likely that they are more important surrounding solar maximum when more active regions are present and temporal variations impact large-scale coronal structure significantly. To fully address this, we must study solutions incorporating the evolution of the photospheric magnetic field (Mikić et al. 1999; Schrijver et al. 2002).

In closing, we reiterate that the main point of this study has been to show that PFSS models are a useful tool for reconstructing the large-scale structure of the solar corona when time-dependent changes in the photospheric flux can be neglected. In reality, however, it is not clear to what extent such conditions exist on the Sun. Finally, we anticipate that the discrepancies between the PFSS and MHD models will increase when vector magnetic field data, such as from the National Solar Observatory's Synoptic Optical Long-term Investigations of the Sun (SOLIS) facility and the Helioseismic and Magnetic Imager (HMI) instrument on the upcoming *Solar Dynamics Observatory* (*SDO*), are incorporated into the MHD boundary conditions.

Workers at SAIC gratefully acknowledge the support of the National Aeronautics and Space Administration (SR&T and SECT Programs) in undertaking this study.

REFERENCES

Altschuler, M. D., & Newkirk, G. 1969, Sol. Phys., 9, 131
Burlaga, L. F., Behannon, K. W., Hansen, S. F., Pneuman, G. W., & Feldman, W. C. 1978, J. Geophys. Res., 83, 4177
Charbonneau, P. 2005, Living Rev. Sol. Phys., 2, 2
de Toma, G. 2006, Observations of Coronal Holes, presented at 2006 Shine Workshop (San Diego: ADNC), http://shadow.adnc.net/shine/Presentations/2006/WG1/GDT/Giuliana_de_Toma_CH_talk06.htm
Fisk, L. A., Schwadron, N. A., & Zurbuchen, T. H. 1998, Space Sci. Rev., 86, 51
Hoeksema, J. T., Wilcox, J. M., & Scherrer, P. H. 1982, J. Geophys. Res., 87, 10331
———. 1983, J. Geophys. Res., 88, 9910
Levine, R. H., Schulz, M., & Frazier, E. N. 1982, Sol. Phys., 77, 363
Linker, J. A., et al. 1999, J. Geophys. Res., 104, 9809
Lionello, R., Linker, J. A., & Mikić, Z. 2001, ApJ, 546, 542
Lionello, R., Mikić, Z., & Linker, J. A. 1998, J. Comput. Phys., Commun., 140, 172
Luhmann, J. G., Li, Y., Arge, C. N., Gazis, P. R., & Ulrich, R. 2002, J. Geophys. Res., 107, 3
Mikić, Z., & Linker, J. A. 1994, ApJ, 430, 898
Mikić, Z., Linker, J. A., & Colborn, J. A. 1996, BAAS, 28, 868
Mikić, Z., Linker, J. A., Schnack, D. D., Lionello, R., & Tarditi, A. 1999, Phys. Plasmas, 6, 2217
Neugebauer, M., Liewer, P. C., Smith, E. J., Skoug, R. M., & Zurbuchen, T. H. 2002, J. Geophys. Res., 107, 13
Neugebauer, M., et al. 1998, J. Geophys. Res., 103, 14587
Parker, E. N. 1958, ApJ, 128, 664
———. 1963, Interplanetary Dynamical Processes (New York: Interscience)
Riley, P., Linker, J. A., & Mikić, Z. 2001, J. Geophys. Res., 106, 15889
———. 2002, J. Geophys. Res., 107, SSH 8-1
Riley, P., Mikić, Z., & Linker, J. A. 2003a, Ann. Geophys., 21, 1347
Riley, P., Mikić, Z., Linker, J., & Zurbuchen, T. H. 2003b, in AIP Conf. Proc. 679, Solar Wind Ten, ed. M. Velli, R. Bruno, & F. Malara (New York: AIP), 79
Roussev, I. I., et al. 2003, ApJ, 595, L57
Schatten, K. H., Wilcox, J. M., & Ness, N. F. 1969, Sol. Phys., 6, 442
Schrijver, C. J., DeRosa, M. L., & Title, A. M. 2002, ApJ, 577, 1006
Schulz, M., Frazier, E. N., & Boucher, D. J. 1978, Sol. Phys., 60, 83
Sheeley, N. R. 2005, Living Rev. Sol. Phys., 2, 5
Smith, S. M., & Schatten, K. H. 1970, BAAS, 2, 345
Uchida, Y., Altschuler, M. D., & Newkirk, G. J. 1973, Sol. Phys., 28, 495
Usmanov, A. V. 1996, in AIP Conf. Proc. 382, Solar Wind Eight, ed. D. Winterhalter (New York: AIP), 141
Wang, Y.-M. 1994, ApJ, 437, L67
Wang, Y.-M., & Sheeley, N. R. 1995, ApJ, 447, L143
———. 2002, J. Geophys. Res., 107, 10
Zhao, X., & Hoeksema, J. T. 1995, J. Geophys. Res., 100, 19
Zhao, X. P., Plunkett, S. P., & Liu, W. 2002, J. Geophys. Res., 107, 13